Bioorganic Chemistry 87 (2019) 417–424

Contents lists available at ScienceDirect

Bioorganic Chemistry

journal homepage: www.elsevier.com/locate/bioorg

NO inhibitory phytochemicals as potential anti-inflammatory agents from the twigs of *Trigonostemon heterophyllus*

Yaru Xi[a,1], Lijun An[a,1], Xueyuan Yang[a], Ziteng Song[a], Jie Zhang[b], Muhetaer Tuerhong[c], Da-Qing Jin[d], Yasushi Ohizumi[e], Dongho Lee[f], Jing Xu[a,*], Yuanqiang Guo[a,*]

[a] State Key Laboratory of Medicinal Chemical Biology, College of Pharmacy, and Tianjin Key Laboratory of Molecular Drug Research, Nankai University, Tianjin 300350, China
[b] Key Laboratory for Green Processing of Chemical Engineering of Xinjiang Bingtuan, School of Chemistry and Chemical Engineering, Shihezi University, Shihezi 832003, China
[c] College of Chemistry and Environmental Sciences, Laboratory of Xinjiang Native Medicinal and Edible Plant Resources Chemistry, Kashgar University, Kashgar 844000, China
[d] School of Medicine, Nankai University, Tianjin 300071, China
[e] Kansei Fukushi Research Institute, Tohoku Fukushi University, Sendai 989-3201, Japan
[f] Department of Biosystems and Biotechnology, College of Life Sciences and Biotechnology, Korea University, Seoul 136-713, Republic of Korea

ARTICLE INFO

Keywords:
NO inhibitors
Trigonostemon heterophyllus
Cleistanthane diterpenoids
Inflammation
Molecular docking

ABSTRACT

Studies on the relationship of nitric oxide (NO) and inflammation have revealed that compounds with NO inhibitory effects are potentially useful for inflammation and related inflammatory disorders. A phytochemical investigation to obtain new NO inhibitors resulted in the isolation of two new cleistanthane diterpenoids (**1** and **2**) and 11 known terpenoids (**3–13**) from *Trigonostemon heterophyllus*. The structures of these terpenoids were established by analysis of their NMR, MS, and electronic circular dichroism (ECD) data. Compounds **1** and **2** possess rare 3,4-*seco*-cleistanthane diterpenoid skeletons. All of the isolates were evaluated biologically for their NO inhibitory effects in lipopolysaccharide (LPS)-induced murine microglial BV-2 cells and compounds **1**, **6**, and **8–10** showed strong NO inhibitory effects with IC_{50} values less than 40 μM. Using Western blotting experiments and molecular docking, the possible mechanism of NO inhibition was investigated.

1. Introduction

Nitric oxide (NO), an important signaling molecule, has been extensively studied and possesses various positive biological functions in multiple tissues of the human body [1,2]. While, NO has also been well known as an inflammatory mediator in numerous studies related to inflammation and overfull NO in tissues has been regarded as a significant sign indicating the inflammatory response of the body, which has been proven to be harmful and can cause a series of subsequent inflammatory and related disorders [2,3]. All of the studies involving NO and related diseases have revealed that NO inhibitors are potentially useful for the development of therapeutical agents to treat inflammation and related disorders [4–6].

The genus *Trigonostemon* Bl., a member of the Euphorbiaceae plant family, contains about 50 species distributed mainly in tropical and subtropical regions of Asia [7]. Some *Trigonostemon* species have been traditionally used as folk medicines for multiple medical indications in Thailand and China [8,9]. Terpenoids, especially diterpenoids, alkaloids, steroids, flavonoids, ligans, coumarins, and phenolics have been reported from this genus and regarded as the major constituents, displaying diverse biological effects, such as cytotoxic, antimicrobial, and antivirus activities [8–20]. The folk medicinal applications of some *Trigonostemon* species and the discovery of bioactive components from some *Trigonostemon* species evoked our great interest in *Trigonostemon* plants [8–10]. As a subordinate species, *Trigonostemon heterophyllus* Merr. is a shrub growing only distributed in Hainan province of China [7], and there is no record on its medicinal purposes in successive Chinese medical books. In our ongoing search for pharmacologically bioactive substances as potential anti-inflammatory agents or lead compounds for inflammatory diseases from plants [21–23], the chemical constituents of the twigs of *T. heterophyllus* were investigated. This investigation led to the isolation of two new 3,4-*seco*-cleistanthane diterpenoids, designated as heterophypenes A and B (**1** and **2**), as well as 11 known terpenoids (**3–13**), from the methanol extract of the twigs

* Corresponding authors.
E-mail addresses: xujing611@nankai.edu.cn (J. Xu), victgyq@nankai.edu.cn (Y. Guo).
[1] These authors contributed equally to this work.

https://doi.org/10.1016/j.bioorg.2019.03.029
Received 29 November 2018; Received in revised form 14 February 2019; Accepted 13 March 2019
Available online 15 March 2019
0045-2068/

of *T. heterophyllus*. The structures of these terpenoids were established by NMR, MS, and electronic circular dichroism (ECD) data analysis. Compounds **1** and **2** possess rare 3,4-*seco*-cleistanthane diterpenoid skeletons. All of the isolates showed inhibitory activities toward lipopolysaccharide (LPS)-induced NO production in murine microglial BV-2 cells. Herein, we describe the structural determination and NO inhibitory effects of these isolated terpenoids as well as their interactions with the inducible nitric oxide synthase (iNOS) protein.

2. Experimental

2.1. General experimental procedures

Optical rotations were recorded on an InsMark IP120 automatic polarimeter (InsMark Instrument Co., Ltd., Shanghai, People's Republic of China). ECD spectra were obtained on a JASCO J-715 CD spectrometer (JASCO Corporation, Tokyo, Japan). Infrared (IR) spectra (KBr disks) were recorded on a Bruker Tensor 27 FT-IR spectrometer. 1D and 2D NMR experiments were performed on a Bruker AV 400 instrument (Bruker, Switzerland, 100 MHz for ^{13}C and 400 MHz for ^{1}H) with TMS as an internal reference at room temperature. ESIMS and HRESIMS data were acquired on a Thermo Finnigan LCQ-Advantage mass spectrometer and an IonSpec 7.0 T FTICR MS (IonSpec Co., Ltd., Lake Forest, CA), respectively. HPLC separations were conducted on a CXTH system, equipped with a Shodex RI-102 detector (Showa Denko Co., Ltd., Tokyo, Japan) and a YMC-pack ODS-AM (20 × 250 mm) column (YMC Co. Ltd., Kyoto, Japan). Medium pressure liquid chromatography (MPLC) was run on a P0100 pump with an ultraviolet (UV) detector (Huideyi Co., Beijing, People's Republic of China) and a column (40 × 400 mm) filled by octadecylsilyl (ODS, 50 μm, YMC Co., Ltd.). Silica gel (200–300 mesh) used for column chromatography was purchased from Qingdao Haiyang Chemical Group Co., Ltd. (Qingdao, People's Republic of China). Chemical reagents (analytical grade) and biological reagents were provided by Tianjin Chemical Reagent Co. (Tianjin, People's Republic of China) and Sigma Co., respectively. The BV-2 cell line was from Shanghai Institutes for Biological Sciences, Chinese Academy of Sciences (Shanghai, People's Republic of China).

2.2. Plant material

The twigs of *T. heterophyllus* were collected from Hainan province, People's Republic of China, in March 2012. The botanical identification was made by one of the authors (Y. Guo), and a voucher specimen (No. 20120310) representing this collection has been deposited in College of Pharmacy, Nankai University, Tianjin, People's Republic of China.

2.3. Extraction and isolation

The twigs of *T. heterophyllus* (8.5 kg) were cut into pieces. After air-drying, the twigs were extracted with MeOH (3 × 60 L) under reflux. The organic solvent was evaporated to afford a crude extract (300 g). The extract was suspended in H_2O (0.4 L) and partitioned with ethyl acetate (3 × 0.4 L). The ethyl acetate soluble-portion (51.5 g) was subjected to silica gel column chromatography (silica gel, 822 g; column, 7 × 50 cm), using a gradient solvent system of petroleum ether-acetone (100: 0, 100: 2, 100: 4, 100: 6, 100: 8, 100: 11, 100: 16, 100: 23, 100: 30, 21 L for each gradient elution) to afford seven fractions (F_1–F_7) according to the TLC analysis. Fraction F_3 was applied to MPLC over octadecylsilane (ODS) eluting with a step gradient from 75 to 94% MeOH in H_2O to give nine subfractions ($F_{3\text{-}1}$–$F_{3\text{-}9}$). Subfraction $F_{3\text{-}8}$ was further purified by preparative HPLC (YMC-pack ODS-AM, 20 × 250 mm, 92% MeOH in H_2O) to afford compounds **1** (t_R = 40 min, 10.6 mg) and **10** (t_R = 28 min, 3.6 mg). The purification of subfraction $F_{3\text{-}4}$ (85% MeOH in H_2O) led to the isolation of compounds **6** (t_R = 43 min, 14 mg) and **9** (t_R = 32 min, 7.3 mg). Fraction F_2 was subjected to the above MPLC to yield four subfractions $F_{2\text{-}1}$–$F_{2\text{-}4}$.

Table 1
^{1}H and ^{13}C NMR spectroscopic data for compounds **1** and **2** ($CDCl_3$, δ in ppm, J in Hz).[a]

Position	1		Position	2	
	^{1}H	^{13}C		^{1}H	^{13}C
1α	1.81 m	27.0, CH_2	1a	1.57 m	31.9, CH_2
1β	1.74 m		1b	1.66 m	
2α	2.68 m	26.3, CH_2	2a	2.29 m	28.1, CH_2
2β	2.55 m		2b	2.52 m	
3		172.3, C	3		179.8, C
4		145.8, C	4		147.4, C
5	2.60 m[b]	44.3, CH	5	2.16 dd (12.5, 2.4)	51.3, CH
6α	1.84 m	27.2, CH_2	6α	1.80 m	28.2, CH_2
6β	1.54 m		6β	1.48 m	
7α	2.22 m	31.5, CH_2	7α	2.31 m	35.3, CH_2
7β	2.49 m		7β	2.06 m	
8		133.9, C	8		137.5, C
9		85.9, C	9	1.90 t (8.4)	43.5, CH
10		38.6, C	10		40.2, C
11α	2.02 m	28.5, CH_2	11α	1.62 m	19.2, CH_2
11β	1.61 m		11β	1.46 m	
12α	1.74 m	31.1, CH_2	12α	1.57 m	35.6, CH_2
12β	1.48 m		12β	1.24 m	
13		39.1, C	13		38.6, C
14	5.44 s	134.2, CH	14	5.20 s	128.8, CH
15	5.68 dd (17.3, 10.4)	145.2, CH	15	5.72 dd (17.2, 10.4)	147.1, CH
16a	4.91 d (17.3)	113.4, CH_2	16a	4.92 d (17.2)	113.0, CH_2
16b	4.99 d (10.4)		16b	4.97 d (10.4)	
17	1.08 s	28.8, CH_3	17	1.01 s	29.3, CH_3
18a	4.79 s	115.1, CH_2	18a	4.73 s	113.7, CH_2
18b	4.98 s		18b	4.87 s	
19	1.80 s	24.0, CH_3	19	1.77 s	23.7, CH_3
20	0.94 s	18.8, CH_3	20	0.79 s	17.3, CH_3

[a] The assignments were based on ^{1}H, ^{13}C, DEPT, HMQC, HMBC, ^{1}H–^{1}H COSY, and NOESY experiments.
[b] Signals are in overlapped regions of the spectra, and the multiplicities could not be discerned.

The subsequent purification of $F_{2\text{-}4}$ (86% MeOH in H_2O) resulted in the isolation of compounds **2** (t_R = 15 min, 2.6 mg) and **13** (t_R = 21 min, 2.4 mg), and the fractionation of subfraction $F_{2\text{-}3}$ (88% MeOH in H_2O) yielded compounds **5** (t_R = 21 min, 35 mg) and **8** (t_R = 19 min, 2.8 mg) with the above HPLC system. Using the same MPLC as applied for the above fractions, F_4 (65–94% MeOH in H_2O) provided subfractions $F_{4\text{-}1}$–$F_{4\text{-}6}$. The purification of subfractions $F_{4\text{-}5}$ (83% MeOH in H_2O) with the above HPLC system resulted in the isolation of compounds **3** (t_R = 34 min, 14.3 mg), **4** (t_R = 31 min, 12.9 mg), and **11** (t_R = 37 min, 2.4 mg). Using the same protocols for the above fractions, fractions F_5 and F_6 yielded subfractions $F_{5\text{-}1}$–$F_{5\text{-}8}$ and $F_{6\text{-}1}$–$F_{6\text{-}7}$. The following is the purification of these subfractions with the above mentioned HPLC. Compound **7** (t_R = 55 min, 19.4 mg) was isolated from $F_{5\text{-}5}$ (83% MeOH in H_2O), and compound **12** (t_R = 30 min, 2.3 mg) was obtained from $F_{6\text{-}2}$ (65% MeOH in H_2O).

2.3.1. Heterophypene A (1)

Colorless oil; $[\alpha]_D^{21}$ −158.3 (*c* 0.2, CH_2Cl_2); ECD (CH_3CN) 196 ($\Delta\varepsilon$ −11.8) nm; IR (film) ν_{max} cm^{-1}: 3079, 2953, 2854, 1728, 1635, 1454, 1436, 1381, 1442, 983; ^{1}H NMR (400 MHz, $CDCl_3$) and ^{13}C NMR (100 MHz, $CDCl_3$) data see Table 1. ESIMS *m/z* 301 $[M+H]^+$; HRESIMS *m/z* 301.2168 $[M+H]^+$, calcd for $C_{20}H_{29}O_2$, 301.2168.

2.3.2. Heterophypene B (2)

Colorless oil; $[\alpha]_D^{21}$ −36.7 (*c* 0.3, CH_2Cl_2); ECD (CH_3CN) 204 ($\Delta\varepsilon$ −3.0) nm; IR (film) ν_{max} cm^{-1}: 3447, 2924, 2856, 1706, 1636, 1455, 1279, 1217, 912, 858; ^{1}H NMR (400 MHz, $CDCl_3$) and ^{13}C NMR (100 MHz, $CDCl_3$) data see Table 1. ESIMS *m/z* 303 $[M+H]^+$; HRESIMS *m/z* 303.2324 $[M+H]^+$, calcd for $C_{20}H_{31}O_2$, 303.2324.

2.4. Computational method

The ECD calculations of the new compounds were performed as previously reported [11,24]. According to the relative configuration of every compound deduced from NOESY spectrum and Chem3D modeling, systematic conformational searches were performed firstly using MOE software and appropriate conformers were selected for geometry optimizations. Geometry optimizations and re-optimizations on the B3LYP/6-31 + G(d,p) level were performed by Gaussian 09 package [25]. The time-dependent density functional theory (TDDFT) ECD calculations for the optimized conformers were carried out at the CAM-B3LYP/SVP level with a CPCM solvent model in acetonitrile, and the calculated ECD spectra of different conformers were simulated with a half bandwidth of ~0.4 eV. The ECD curves were extracted by SpecDis 1.62 software [26]. The overall ECD curves of all the compounds were weighted by Boltzmann distribution after UV correction.

2.5. Bioassay for anti-inflammatory effects

The anti-inflammatory effects of compounds were examined by inhibiting NO release in LPS-induced murine microglial BV-2 cells. The cells were cultured at 37 °C in DMEM supplemented with 10% (*v/v*) inactivated fetal bovine serum and 100 U/mL penicillin/streptomycin under a water-saturated atmosphere of 95% air and 5% CO_2. BV-2 cells were seeded in 96-well culture plates (5×10^4 cells/well) and allowed to adhere for 24 h at 37 °C. The cells were incubated for 20 h with or without 0.20 μg/mL of LPS (Sigma Chemical Co., St. Louis, MO, U.S.A.) in the absence or presence of the test compounds. 2-Methyl-2-thiopseudourea, sulfate (SMT) was used as a positive control. As a parameter of NO synthesis, the nitrite concentration in the culture supernatant was measured by the Griess reaction. Briefly, 50 μL of the cell culture supernatant were reacted with 50 μL of Griess reagent [1:1 mixture of 0.1% *N*-(1-naphtyl)ethylenediamine in H_2O and 1% sulfanilamide in 5% phosphoric acid] in a 96 well plate and the absorbance was read on a Multiskan MK3 microplate reader (Thermo Fisher Scientific Inc., Waltham, MA, USA). The amount of nitrite was calculated using a standard curve of known nitrite concentration versus absorbance at 550 nm. The IC_{50} values were determined using the software SPSS11.5 from the corresponding experiments performed in triplicate.

2.6. Western blotting analysis

BV-2 cells were seeded in six-well plates at the density of 1×10^6 cells/well for 24 h. Then, the cells were pretreated with compound **10** for 30 min and stimulated with LPS (0.2 μg/mL) for 24 h. The cells were washed with cold PBS twice. After collecting, the cells were lysed by lysis buffer with freshly added protease inhibitor cocktail and phenymethyl sulfonylfluoride. Then, the lysates were centrifuged at 10,000 rpm for 10 min and the supernatants were collected to acquire the total protein. The protein concentration was determined by the BCA protein assay kit. (Solarbio, Beijing, People's Republic of China). Approximate 20 μg of proteins were separated by 10% SDS-PAGE and then transferred to PVDF membranes. The membranes were blocked in 15% skim milk for 2 h at room temperature and incubated with primary antibodies overnight at 4 °C. After being washed with TBST for 30 min, the membranes were incubated with secondary antibody (diluted 1: 5000 in 5% skim milk) for 1 h at room temperature and then washed with TBST for 30 min. Lastly, the protein blots were visualized using an ECL detection kit. (Beyotime, Shanghai, People's Republic of China). *β*-Actin protein was used as internal reference. Each band was quantified by Image-J software.

2.7. Molecular docking studies

Molecular docking simulations were performed using the software AutoDock Vina along with AutoDock Tools (ADT 1.5.6) using the hybrid Lamarckian Genetic Algorithm (LGA) [27,28]. The three dimensional (3D) crystal structure of iNOS (PDB code 3E6T) was obtained from the RCSB Protein Data Bank, which resolution was 2.5 Å [29]. The standard 3D structures (PDB format) of selected compounds for molecular docking were constructed by chem3D Pro 14.0 software, whose configurations were determined by their NOESY spectra and Chem3D modeling. The cubic grid box of 20 Å size (x, y, z) with a spacing of 1.000 Å and grid maps were built [28,29]. All of the other parameters were used according to default settings of AutoDock Vina. Results differing by less than 2.0 Å in positional root mean-square deviation (RMSD) were clustered together, and the results of the most favorable free energy of binding were chosen as the resultant complex structures.

3. Results and discussion

3.1. Structure elucidation

Compound **1** was obtained as a colorless oil. Its molecular formula was determined as $C_{20}H_{28}O_2$ based on the ^{13}C NMR data and the HRESIMS ion at *m/z* 301.2165 $[M+H]^+$ (calcd for $C_{20}H_{29}O_2$, 301.2168). The ^1H NMR data of **1** (Table 1) displayed signals assignable to two aliphatic methyl singlets (δ_H 1.08 and 0.94), one olefinic methyl singlet (δ_H 1.80), six olefinic protons [δ_H 5.68 (1H, dd, J = 17.3, 10.4 Hz), 5.44 (1H, s), 4.99 (1H, d, J = 10.4 Hz), 4.98 (1H, s), 4.91 (1H, d, J = 17.3 Hz), and 4.79 (1H, s)]. The ^{13}C NMR data of **1** (Table 1) showed 20 resonances comprising three methyls, eight methylenes [two olefinic methylenes (δ_C 115.1 and 113.4)], three methines [two olefinic methines (δ_C 134.2 and 145.2)], and six quaternary carbons [one carbonyl (δ_C 172.3), one oxygenated tertiary carbon (δ_C 85.9), and two olefinic carbons (δ_C 133.9 and 145.9)] (Table 1) with the aid of DEPT and HMQC experiments. The above spectroscopic features and the 20 skeletal carbons in the ^{13}C NMR spectrum indicated compound **1** to be a diterpenoid [30–32]. The following HMBC and ^1H–^1H COSY experiments enabled this diterpenoid structure to be elucidated. From the HMBC spectrum, the long-range correlations of H_3-17 to C-12–C-15, H-14 to C-8, C-9, C-12, C-13, C-15 and C-17, H-15 to C-12–C-14, C-16, and C-17, and H_2-16 to C-13 and C-15, together with ^1H–^1H COSY couplings (Fig. 2) indicated the presence of an unsaturated six-membered ring B with a methyl group (Me-17) and a vinyl group (−CH=CH_2) both attached at C-13. Correspondingly, the oxygenated tertiary carbon signal at δ_C 85.9 and olefinic signals at δ_C 133.9 and 134.2 were attributed to C-9, C-8, and C-14, respectively. In addition to this six-membered ring, the other six-membered ring A with a methyl group (Me-20) attached at C-10 and an isopropenyl group at C-5 was also inferred from the ^1H–^1H COSY correlations of H-5/H_2-6/H_2-7 and the HMBC couplings of H_3-20 to C-5, C-9, and C-10, H-5 to C-4, C-6, C-7, C-9, C-10, C-18, and C-19, H_3-19 to C-4, C-5 and C-18, and H_2-18 to C-4, C-5 and C-19 (Fig. 2). The two six-membered rings A and B were fused by sharing C-8 and C-9. After assigning the carbon signals in the above moieties, there were three carbon signals left including a carbonyl (δ_C 172.3) and two methylenes (δ_C 27.0 and 26.3), which constituted a three-carbon unit to be attached at C-10 by interpretation of the 1D and 2D NMR data (Fig. 2). The structure of **1** seemed to be established based on the above analysis. However, the molecular formula deduced from the above NMR spectroscopic data was inconsistent with the HRESIMS data. The total indices of hydrogen deficiency from the HRESIMS data suggested one more ring in this compound. According to the chemical shifts of the carbonyl (δ_C 172.3) and the oxygenated quaternary carbon (δ_C 85.9), the one more ring in this compound could only be 3,9-lactone ring formed by the carboxyl group (C-3) and the C-9 hydroxy group (Fig. 2) [33,34]. All of the above evidence allowed the planar structure of compound **1** to be established as shown in Fig. 1, which is a rare 3,4-*seco*-cleistanthane diterpenoid-3,9-lactone.

The relative configuration of compound **1** was elucidated using NOESY experiment and chem3D modeling. The NOESY interactions observed for H_3-20/H-12*α*, H_3-20/H-6*α*, H-5/H-7*β*, H-7*α*/H-14, H-1*α*/

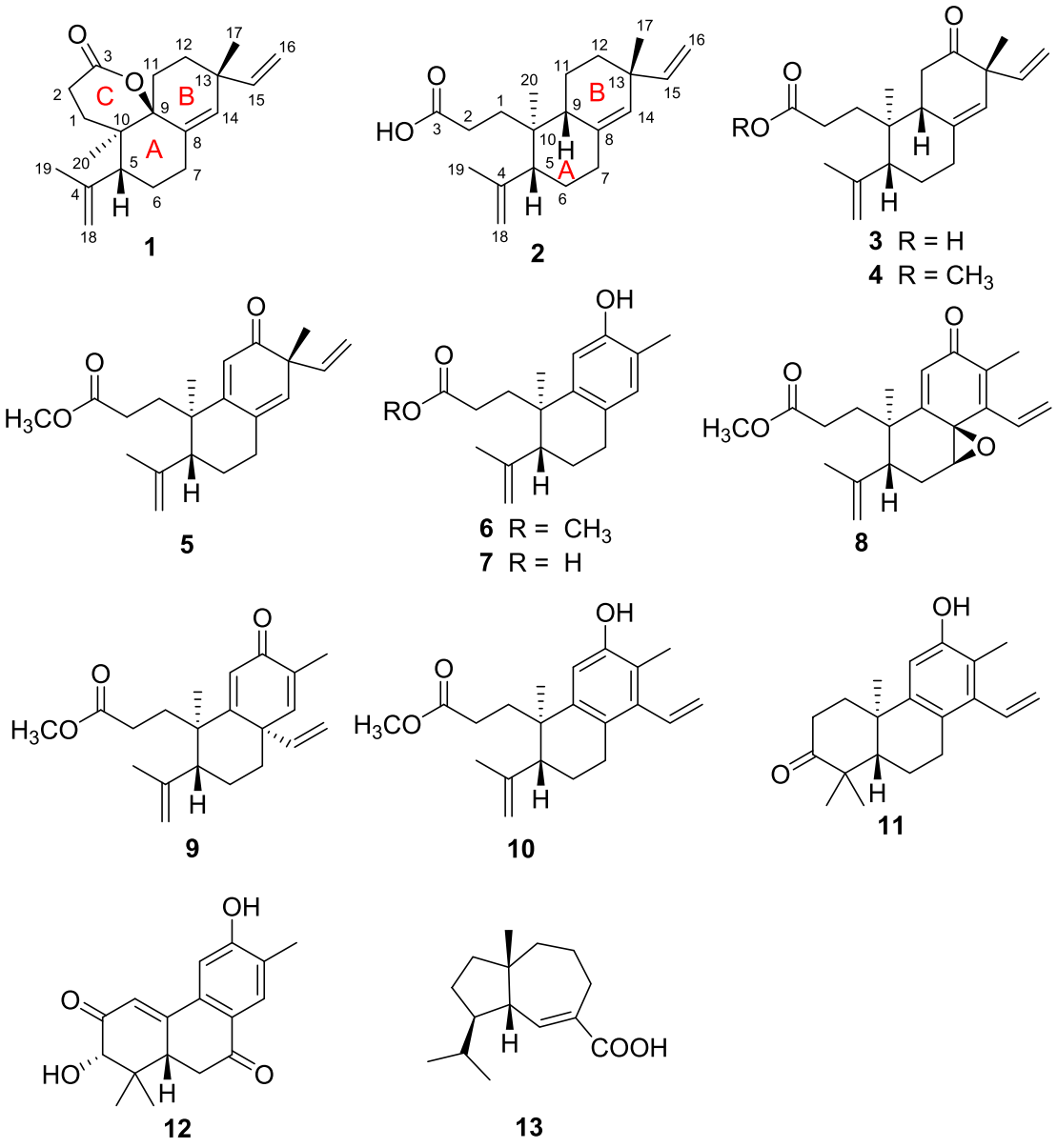

Fig. 1. Structures of compounds **1–13**.

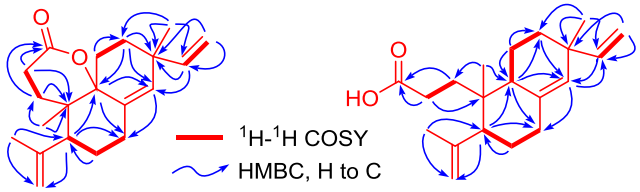

Fig. 2. ^{1}H–^{1}H COSY and key HMBC correlations of compounds **1** and **2**.

H-11α, H-11β/H$_3$-17, and H-12β/H$_3$-17 (Fig. 3), along with Chem3D modeling, revealed a molecular conformation as depicted in Fig. 3. In this molecular arrangement of **1**, ring A existed in a chair conformation with H-5 β-axially oriented and Me-20 α-axially oriented, ring B presented a twist-chair conformation with Me-17 in a β-position, and ring C presented a normal chair conformation and was *cis*-fused with the ring A. Following the definition of the relative configuration, time-dependent density functional theory (TDDFT) ECD calculations, a powerful tool to assign the absolute configurations of natural products [35,36], were applied to determine the absolute configuration of compound **1**. After systematic conformational searches, geometry optimizations, and TDDFT calculations, the ECD spectra were extracted using SpecDis 1.62 software. The calculated ECD spectrum of **1** (Fig. 4) accorded with the experimental data closely, pointing to an absolute configuration of 5*R*, 9*S*, 10*R*, and 13*R* for **1**. Compound **1** was therefore elucidated and has been given a trivial name heterophypene A.

Compound **2** was obtained as a colorless oil. Its molecular formula was deduced as $C_{20}H_{30}O_2$ from the ^{13}C NMR and HRESIMS ion at *m/z* 303.2324 $[M+H]^+$ (calcd for $C_{20}H_{31}O_2$, 303.2324). The ^{1}H NMR data for **2** (Table 1) displayed signals attributable to two aliphatic methyl singlets (δ_H 0.79 and 1.01), one olefinic methyl singlet (δ_H 1.77), six olefinic protons [δ_H 5.72 (1H, dd, J = 17.2, 10.4 Hz), 5.20 (1H, s), 4.97 (1H, d, J = 10.4 Hz), 4.92 (1H, d, J = 17.2 Hz), 4.87 (1H, s), and 4.73 (1H, s)]. Corresponding to these olefinic protons, six olefinic carbons (δ_C 113.0, 113.7, 128.8, 137.5, 147.1, and 147.4) were observed in the ^{13}C NMR spectrum of **2** (Table 1). The above ^{1}H and ^{13}C NMR spectroscopic features were almost identical to those of compound **1**, suggesting that compound **2** should also be diterpenoid structurally related to compound **1**. Comparison of their NMR data revealed the main differences between compounds **1** and **2**. It was found that the carbonyl signal in **1** shifted downfield by about 7 ppm in compound **2** [δ_C 172.3

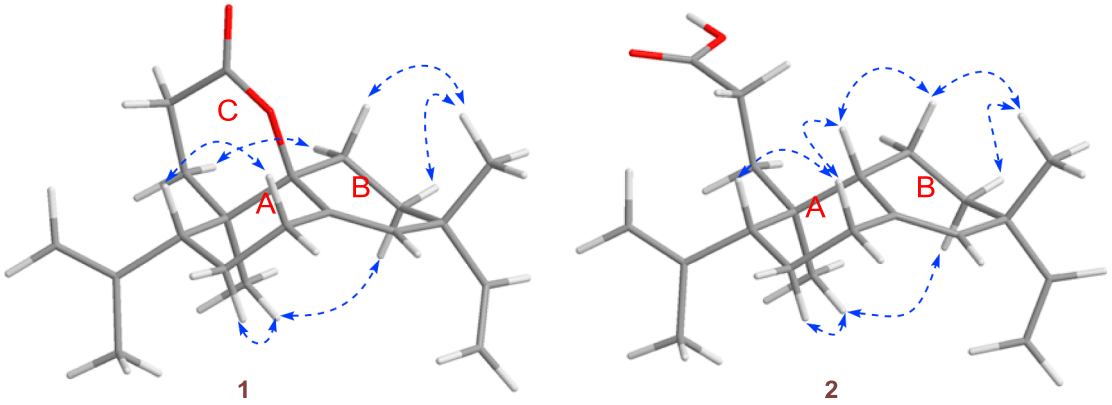

Fig. 3. Conformations and key NOESY correlations of compounds **1** and **2**.

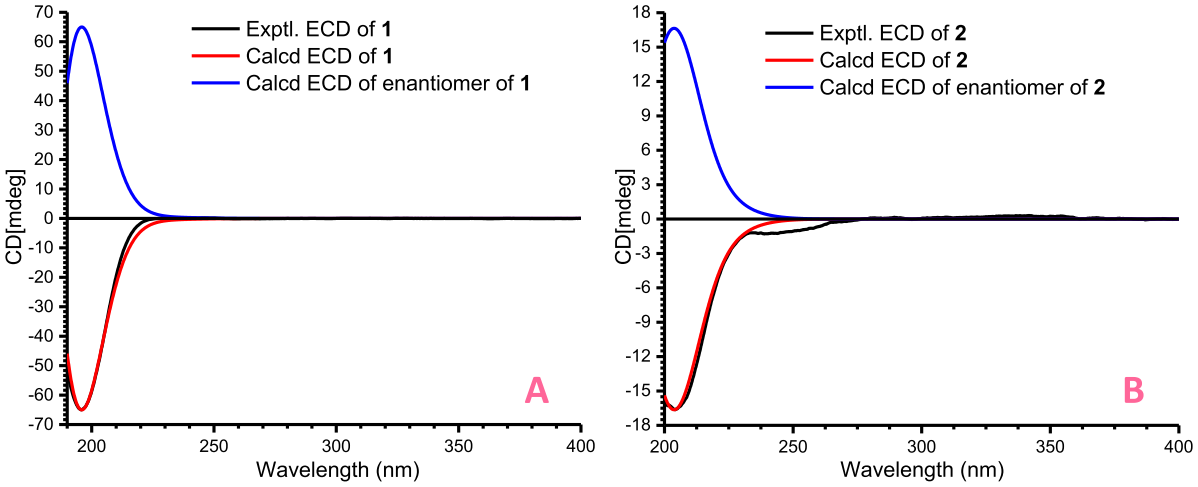

Fig. 4. Calculated and experimental ECD spectra of compounds **1** (A) and **2** (B) in acetonitrile.

(C-3) in **1**; δ_C 179.8 (C-3) in **2**], which implied that lactone ring in compound **1** was cleaved to be a carboxyl group in **2**. In addition, the oxygenated quaternary carbon at δ_C 85.9 (C-9) in compound **1** disappeared and one more aliphatic methine appeared in **2**, suggesting that the oxygenated tertiary carbon [δ_C 85.9 (C-9)] in **1** was deoxidized to be an aliphatic methine [δ_C 43.5 (C-9)] in **2** (Table 1). These deductions were substantiated by the following DEPT, HMQC, HMBC, and ^{1}H–^{1}H COSY experiments (Fig. 2), and the interpretation of 1D and 2D NMR spectroscopic data led to the assignments of all the proton and carbon signals. The planar structure of compound **2** was thus established to be as shown in Fig. 2.

After defining the planar structure, a NOESY experiment enabled the relative configuration of **2** to be elucidated. The NOESY interactions observed for H_3-20/H-12α, H_3-20/H-6α, H-5/H-7β, H-5/H-9, H-7β/H-9, H-9/H-11β, H-7α/H-14, H_3-17/H-11β, and H_3-17/H-12β (Fig. 3), together with Chem3D modeling, revealed a molecular conformation as depicted in Fig. 3. In this molecular arrangement of compound **2**, ring A existed in a chair conformation with H-5 β-axially oriented and Me-20 α-axially oriented, ring B presented a twist-chair conformation with Me-17 in a β-position, and H-9, relative to the 6/6 fused bicyclic rings A and B, was β-axially oriented. As in the case of **1**, the absolute configuration of **2** was determined by comparison of experimental and calculated ECD spectra, of which the latter was obtained by performing TDDFT ECD calculations. The calculated ECD spectrum matched the experimental data closely (Fig. 4), suggesting the absolute configuration of **2** to be 5*R*, 9*R*, 10*R*, and 13*R* (Fig. 4). On the basis of the above analysis, the structure of compound **2** was elucidated and given a trivial name heterophypene B.

In addition to the new diterpenoids, 11 known terpenoids were also isolated from the twigs of *T. heterophyllus*. By analysis of their NMR spectroscopic data and comparison of the data with those reported in the literature, the known compounds were identified as howpene B (**3**) [11], howpene C (**4**) [11], trigoflavidone A (**5**) [37], trigoheteric acid methyl ester (**6**) [20], 3,4-*seco*-sonderianic acid (**7**) [38], trigonochinene D (**8**) [39], trigoflavidone D (**9**) [37], 3,4-*seco*-sonderianol (**10**) [40], sonderianol (**11**) [40], trigoxyphins G (**12**) [41], and howpene A (**13**) [11].

3.2. Anti-inflammatory activities indicated by inhibiting LPS-induced NO production

Accumulating studies have revealed that inflammation and related diseases have a close relationship with excessive NO in tissues and compounds with NO inhibitory effects may be useful for the treatment of inflammation and related neurodegenerative diseases [3-6]. To obtain new NO inhibitors as potential lead compounds or anti-inflammatory agents for inflammatory diseases, compounds **1–13** were thus tested for their NO inhibitory effects according to the method described previously [42,43]. The NO inhibitor, 2-methyl-2-thiopseudourea, sulfate (SMT), was used as positive control (IC_{50} value of 4.2 μM) [21,22]. After treated with compounds and stimulated with LPS for 24 h, the amounts of NO production in the supernatant of BV-2 cells were measured, which were shown in Fig. 5. All of the isolates exhibited NO inhibitory effects in LPS-induced murine microglial BV-2 cells and compounds **1**, **6**, and **8–10** exerted more inhibition against NO production, whose IC_{50} values were less than 40 μM (Table 2). The cytotoxic test (MTT assay) showed that all of the isolates had no impact on BV-2 cell survival at their effective concentrations (data not shown).

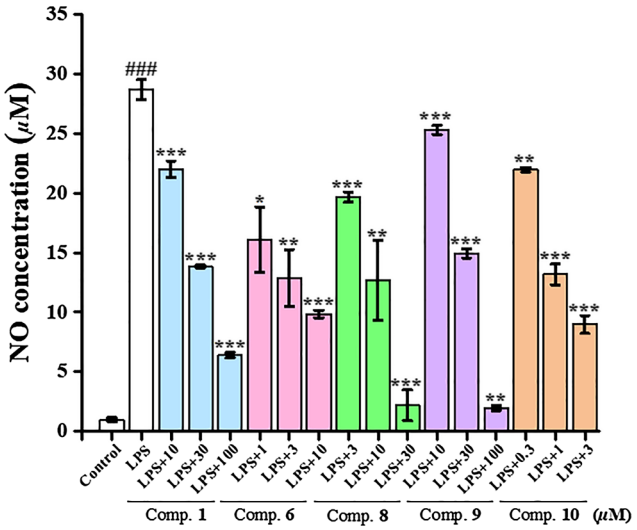

Fig. 5. Effects of compounds **1**, **6**, and **8–10** on NO production in LPS-induced BV-2 cells. BV-2 cells were pretreated with five compounds for 30 min, then cells were stimulated with LPS (0.2 μg/mL) for 24 h. The amounts of NO in the supernatant were measured. Data were obtained at least three independent experiments. $^{\#\#\#}p < 0.001$, significantly different from LPS-untreated sample, $^{*}p < 0.05$, $^{**}p < 0.01$, $^{***}p < 0.001$, significantly different from LPS-treated sample.

Table 2
IC_{50} values of compounds 1–13 inhibiting NO production in BV-2 cells.

Compound	IC_{50} (μM)	Compound	IC_{50} (μM)
1	34.5 ± 1.1	**8**	9.5 ± 2.0
2	51.0 ± 2.5	**9**	28.4 ± 0.58
3	> 30	**10**	1.5 ± 0.3
4	> 30	**11**	55.5 ± 1.03
5	35.6 ± 0.67	**12**	> 30
6	2.8 ± 0.3	**13**	> 30
7	> 30	SMT[a]	4.2 ± 0.2

[a] SMT(2-Methyl-2-thiopseudourea, sulfate) was used as a positive control. Data are presented based on three experiments.

3.3. Effects on iNOS protein expression

As well known, NO is a crucial pro-inflammatory mediator and plays an important role in inflammatory related diseases. The amount of NO production in the inflammatory process is regulated mainly by iNOS. To better understand the NO inhibitory mechanism, the most active compound **10** was selected to investigate the effects on the iNOS protein expression using Western blotting experiments. As shown in Fig. 6, the levels of iNOS protein increased with LPS stimulation, and decreased in a dose-dependent manner by treatment with compound **10**. These results suggested that compound **10** could inhibit NO production by suppression of iNOS expression.

3.4. Interactions of bioactive compounds with iNOS protein

To understand the interactions between bioactive compounds and iNOS, molecular docking studies were applied to evaluate the binding ability and sites of these bioactive diterpenoids with the iNOS protein [44–46]. The more bioactive compounds (**1**, **6**, and **8–10**) with significant NO inhibitory effects (IC_{50} values < 40 μM) were selected to perform molecular docking. Results from molecular docking studies revealed that compounds **1**, **6**, and **8–10** had strong interactions with the iNOS protein (Fig. 7). The logarithms of free binding energy and the binding residues are shown in Table 3. The results of molecular docking implied that the possible mechanism of NO inhibition of these bioactive

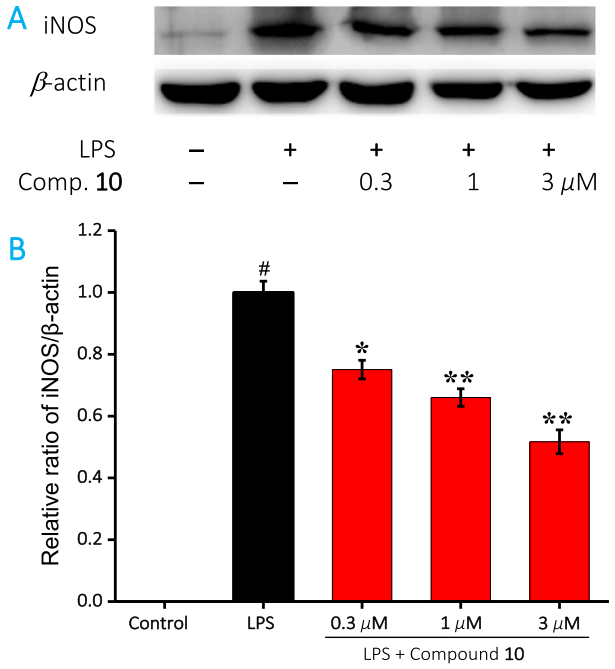

Fig. 6. Effects of compound **10** on LPS-induced iNOS protein expression in BV-2 cells. BV-2 cells were pre-treated with compound **10** for 30 min, then stimulated by LPS (0.2 μg/mL) for 24 h, and Western blotting analysis was performed. (A) Western blotting results of iNOS protein levels. (B) Quantitative analysis of iNOS protein expression. β-Actin protein was used as internal reference. $\#p < 0.001$ compared with LPS-untreated cells, $^{**}p < 0.01$, $^{*}p < 0.05$ compared with LPS-stimulated cells. Data were obtained by at least three independent experiments.

terpenoids is to interact with the iNOS protein by targeting residues of the active cavities of iNOS protein.

4. Conclusion

The present phytochemical investigation on *T. heterophyllus* led to the isolation of 13 terpenoid including two new ones. The structures were elucidated on the basis of extensive 1D and 2D NMR spectroscopic data analysis, and the absolute configurations of compounds **1** and **2** were established by experimental and calculated ECD spectra. All of the isolates exhibited NO inhibitory effects in LPS-induced murine microglial BV-2 cells. Compared to the other compounds, compounds **1**, **6**, and **8–10** exerted more inhibition against NO production, whose IC_{50} values were less than 40 μM. Western blotting experiments revealed that compound **10**, the most active compound, exhibited the anti-inflammatory effects by down-regulating the iNOS protein expression. Molecular docking revealed that compounds **1**, **6**, and **8–10** had strong interactions with the iNOS protein by targeting residues of the active cavities of iNOS, disclosing that the possible mechanism of bioactive compounds with NO inhibitory effects. The discovery of bioactive terpenoids suggested that the plant *T. heterophyllus* has the potential medicinal value for treatment of inflammation. While, the more bioactive compounds, especially compounds **6** and **10** (IC_{50} values, 2.8 and 1.5 μM, respectively), may have the potential to be developed as anti-inflammatory agents for various inflammatory diseases and other related disorders [4–6].

Conflict of interest

The authors of the present manuscript have declared that no competing interests exist.

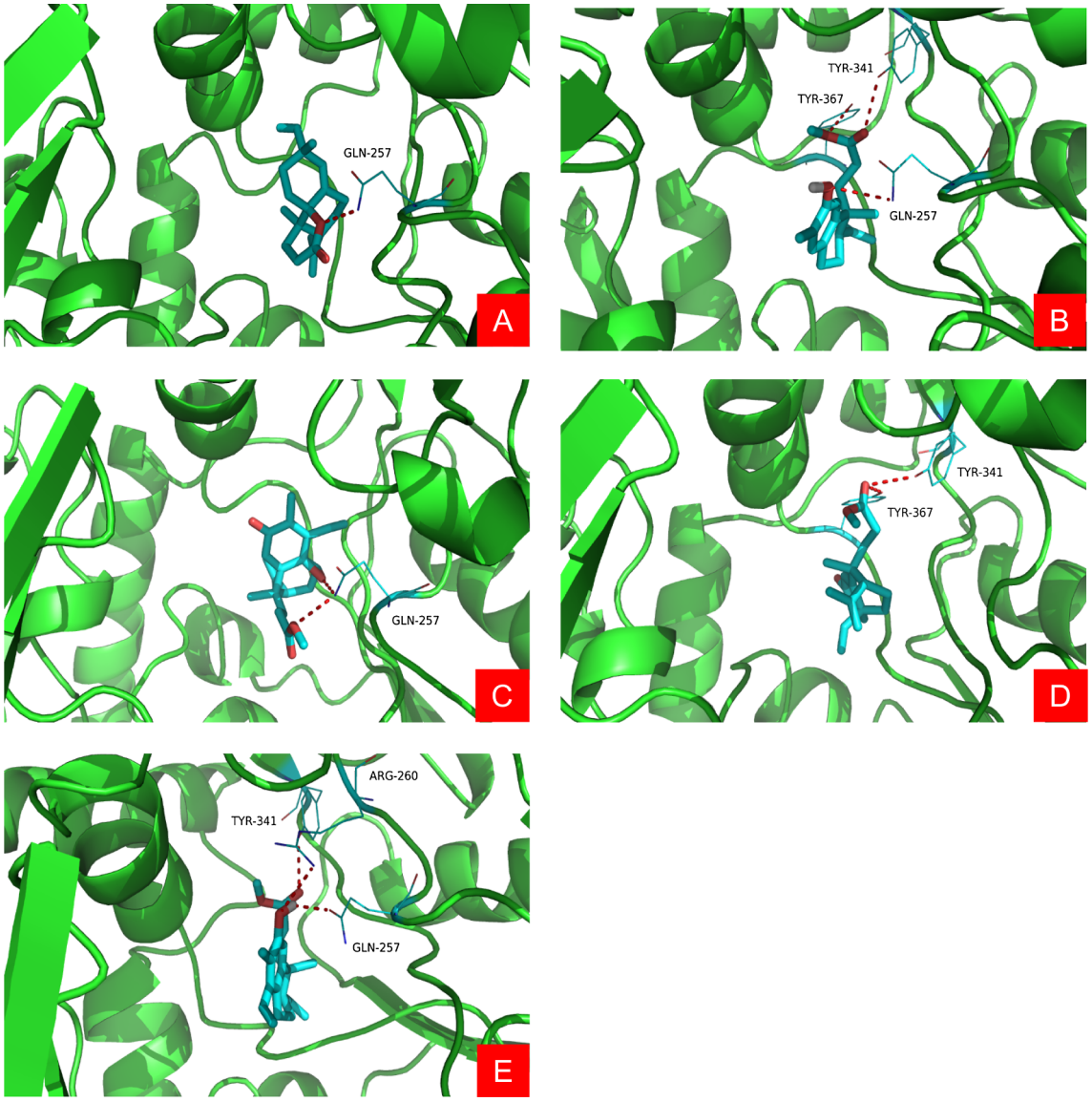

Fig. 7. Molecular docking simulations obtained at the lowest energy conformation, highlighting potential hydrogen contacts of compounds **1** (A), **6** (B), and **8–10** (C–E), respectively. (Colored by atom: carbon is cyan; nitrogen is blue; oxygen is red; hydrogen is gray; sulfur is orange). For clarity, only interacting residues are labeled. Hydrogen bonding interactions are shown by dashes. These figures were created by PyMOL.

Table 3
Logarithms of free binding energies (FBE, kcal/mol) of compounds **1**, **6**, and **8–10** to the active cavities of iNOS (PDB code, 3E6T) and targeting residues of the binding site located on the mobile flap.

Compound	−Log (FBE)	Targeting residues
1	−8.5	GLN-257
6	−8.5	TYR-341 TYR-367 GLN-257
8	−8.0	GLN-257
9	−7.5	TYR-341 TYR-367
10	−7.7	TYR-341 GLN-257 ARG-260

Acknowledgments

This research was supported by the National Key Research and Development Program of China (No. 2018YFA0507204), Hundred Young Academic Leaders Program of Nankai University, the Natural Science Foundation of Tianjin, China (No. 16JCYBJC27700), National Natural Science Foundation of China (Nos. U1703107, 21642016, and 21372125), and State Key Laboratory for Chemistry and Molecular Engineering of Medicinal Resources (Guangxi Normal University, No. CMEMR2018-B02).

Appendix A. Supplementary material

Supplementary data to this article can be found online at https://doi.org/10.1016/j.bioorg.2019.03.029.

References

[1] D.S. Bredt, S.H. Snyder, Annu. Rev. Biochem. 63 (1994) 175–195.
[2] U. Förstermann, H. Li, Nitric oxide: biological synthesis and functions, in: A. Hermann, G. Sitdikova, T. Weiger (Eds.), Gasotransmitters: Physiology and Pathophysiology, Springer, Berlin, Heidelberg, 2012, pp. 1–36.
[3] J.N. Sharma, A. Al-Omran, S.S. Parvathy, Inflammopharmacology 15 (2007) 252–259.
[4] S. Shadfar, C.J. Hwang, M.S. Lim, D.Y. Choi, T.H. Jin, Arch. Pharm. Res. 38 (2015) 2106–2119.
[5] K.H. Kim, S.K. Ha, S.U. Choi, S.Y. Kim, K.R. Lee, Planta Med. 79 (2013) 361–364.
[6] H. Wang, Y. Liu, J. Zhang, J. Xu, C.A. Cui, Y. Guo, D.Q. Jin, Neurosci. Lett. 612 (2017) 149–154.
[7] Editorial Committee of the Flora of China, Chinese Academy of Sciences, Flora of China, vol. 44 (2), Science Press, Beijing, 1999, pp. 162−164.

[8] Y.G. Chen, J.C. Wu, G.Y. Chen, C.R. Han, X.P. Song, Chem. Biodivers. 8 (2011) 1958–1967.
[9] J.B. Xu, J.M. Yue, Org. Chem. Front. 1 (2014) 1225–1252.
[10] Y.P. Liu, S. Hu, Q. Wen, Y.L. Ma, Z.H. Jiang, J.Y. Tang, Y.H. Fu, Bioorg. Chem. 79 (2018) 107–110.
[11] J. Ma, X. Yang, P. Wang, B. Dong, G. Su, M. Tuerhong, D.Q. Jin, J. Xu, D. Lee, Y. Ohizumi, J. Lin, Y. Guo, Bioorg. Chem. 75 (2017) 71–77.
[12] K. Praphakorn, C. Ratchanaporn, P. Samran, K. Palangpon, C. Warangkana, U. Tanyarath, C. Walee, S. Apichart, Tetrahedron 73 (2017) 1594–1601.
[13] J. Xu, M. Peng, X. Sun, X. Liu, L. Tong, G. Su, Y. Ohizumi, D. Lee, Y. Guo, Bioorg. Med. Chem. Lett. 26 (2016) 4785–4789.
[14] Y.Q. Liu, Y.T. Di, Y.H. Wang, X.J. Hao, X.J. Hu, Helv. Chim. Acta 99 (2016) 558–561.
[15] Y.B. Zeng, S.S. Ma, Z.K. Guo, B. Jiang, W.L. Mei, H.F. Dai, Nat. Prod. Commun. 11 (2016) 369–370.
[16] B. Yang, Z. Meng, Z. Li, L. Sun, Y. Hu, Z. Wang, G. Ding, W. Xiao, C. Han, Phytochem. Lett. 11 (2015) 270–274.
[17] S.S. Ma, W.L. Mei, Z.K. Guo, S.B. Liu, Y.X. Zhao, D.L. Yang, Y.B. Zeng, B. Jiang, H.F. Dai, Org. Lett. 15 (2013) 1492–1495.
[18] M. Bourjot, P. Leyssen, J. Neyts, V. Dumontet, M. Litaudon, Molecules 19 (2014) 3617–3627.
[19] Y.Y. Cheng, H. Chen, H.P. He, Y. Zhang, S.F. Li, G.H. Tang, L.L. Guo, W. Yang, F. Zhu, Y.T. Zheng, S.L. Li, X.J. Hao, Phytochemistry 96 (2013) 360–369.
[20] S.H. Dong, H.B. Liu, C.H. Xu, J. Ding, J.M. Yue, J. Nat. Prod. 74 (2011) 2576–2581.
[21] F. Liu, B. Dong, X. Yang, Y. Yang, J. Zhang, D.Q. Jin, Y. Ohizumi, D. Lee, J. Xu, Y. Guo, Bioorg. Chem. 77 (2018) 168–175.
[22] P. Wang, X. Yang, F. Liu, Y. Liang, G. Su, M. Tuerhong, D.Q. Jin, J. Xu, D. Lee, Y. Ohizumi, Y. Guo, Bioorg. Chem. 76 (2018) 53–60.
[23] X. Cao, X. Yang, P. Wang, Y. Liang, F. Liu, M. Tuerhong, D.Q. Jin, J. Xu, D. Lee, Y. Ohizumi, Y. Guo, Bioorg. Chem. 75 (2017) 139–148.
[24] J. Xu, F. Ji, X. Sun, X. Cao, S. Li, Y. Ohizumi, Y. Guo, J. Nat. Prod. 78 (2015) 2648–2656.
[25] M.J. Frisch, G.W. Trucks, H.B. Schlegel, G.E. Scuseria, M.A. Robb, J.R. Cheeseman, G. Scalmani, V. Barone, B. Mennucci, G.A. Petersson, H. Nakatsuji, M. Caricato, X. Li, H.P. Hratchian, A.F. Izmaylov, J. Bloino, G. Zheng, J.L. Sonnenberg, M. Hada, M. Ehara, K. Toyota, R. Fukuda, J. Hasegawa, M. Ishida, T. Nakajima, Y. Honda, O. Kitao, H. Nakai, T. Vreven, J.A. Montgomery Jr., J.E. Peralta, F. Ogliaro, M. Bearpark, J.J. Heyd, E. Brothers, K.N. Kudin, V.N. Staroverov, R. Kobayashi, J. Normand, K. Raghavachari, A. Rendell, J.C. Burant, S.S. Iyengar, J. Tomasi, M. Cossi, N. Rega, J.M. Millam, M. Klene, J.E. Knox, J.B. Cross, V. Bakken, C. Adamo, J. Jaramillo, R. Gomperts, R.E. Stratmann, O. Yazyev, A.J. Austin, R. Cammi, C. Pomelli, J.W. Ochterski, R.L. Martin, K. Morokuma, V.G. Zakrzewski, G.A. Voth, P. Salvador, J.J. Dannenberg, S. Dapprich, A.D. Daniels, O. Farkas, J.B. Foresman, J.V. Ortiz, J. Cioslowski, D.J. Fox, Gaussian 09, Revision A.02, Gaussian, Inc., Wallingford, CT, 2009.
[26] T. Bruhn, A. Schaumlöffel, Y. Hemberger, G. Bringmann, SpecDis, Version 1.62, University of Wuerzburg, Germany, 2014.
[27] M.A. Loza-Mejía, J.R. Salazar, J. Mol. Graph. Model. 62 (2015) 18–25.
[28] J. Xu, M. Wang, X. Sun, Q. Ren, X. Cao, S. Li, Y. Ohizumi, Y. Guo, J. Nat. Prod. 79 (2016) 2924–2932.
[29] E.D. Garcin, A.S. Arvai, R.J. Rosenfeld, M.D. Kroeger, B.R. Crane, G. Andersson, G. Andrews, P.J. Hamley, P.R. Mallinder, D.J. Nicholls, S.A. St-Gallay, A.C. Tinker, N.P. Gensmantel, A. Mete, D.R. Cheshire, S. Connolly, D.J. Stuehr, A. Åberg, A.V. Wallace, J.A. Tainer, E.D. Getzoff, Nat. Chem. Biol. 4 (2008) 700–707.
[30] E. Bautista, R.A. Toscano, A. Ortega, J. Nat. Prod. 77 (2014) 1088–1092.
[31] C.S. Kim, L. Subedi, S.Y. Kim, S.U. Choi, K.H. Kim, K.R. Lee, J. Nat. Prod. 79 (2016) 387–394.
[32] J. Xu, J. Kang, X. Sun, X. Cao, K. Rena, D. Lee, Q. Ren, S. Li, Y. Ohizumi, Y. Guo, J. Nat. Prod. 79 (2016) 170–179.
[33] M.M. Farimani, S. Taheri, S.N. Ebrahimi, M.B. Bahadori, H.R. Khavasi, S. Zimmermann, R. Brun, M. Hamburger, Org. Lett. 14 (2012) 166–169.
[34] M.M. Farimani, S.N. Ebrahimi, P. Salehi, M.B. Bahadori, A. Sonboli, H.R. Khavasi, S. Zimmermann, M. Kaiser, M. Hamburger, J. Nat. Prod. 76 (2013) 1806–1809.
[35] X.C. Li, D. Ferreira, Y. Ding, Curr. Org. Chem. 14 (2010) 1678–1697.
[36] C.P. Sun, A.G. Kutateladze, F. Zhao, L.X. Chen, F. Qiu, Org. Biomol. Chem. 15 (2017) 1110–1114.
[37] G.H. Tang, H.P. He, Y.C. Gu, Y.T. Di, Y.H. Wang, S.F. Li, S.L. Li, Y. Zhang, X.J. Hao, Tetrahedron 68 (2012) 9679–9684.
[38] X.J. Hu, Y.H. Wang, L.Y. Kong, H.P. He, S. Gao, H.Y. Liu, J. Ding, H. Xie, Y.T. Di, X.J. Hao, Tetrahedron Lett. 50 (2009) 2917–2919.
[39] S. Yin, Z.S. Su, Z.W. Zhou, L. Dong, J.M. Yue, J. Nat. Prod. 71 (2008) 1414–1417.
[40] A.A. Craveiro, E.R. Silveira, Phytochemistry 21 (1982) 2571–2574.
[41] B.D. Lin, M.L. Han, Y.C. Ji, H.D. Chen, S.P. Yang, S. Zhang, M.Y. Geng, J.M. Yue, J. Nat. Prod. 73 (2010) 1301–1305.
[42] S.R. Lee, S. Lee, E. Moon, H.J. Park, H.B. Park, K.H. Kim, Bioorg. Chem. 70 (2017) 94–99.
[43] F. Liu, X. Yang, J. Ma, Y. Yang, C. Xie, M. Tuerhong, D.Q. Jin, J. Xu, D. Lee, Y. Ohizumi, Y. Guo, Bioorg. Chem. 75 (2017) 149–156.
[44] W. Zhao, Z. Sun, S. Wang, Z. Li, L. Zheng, Inflammation 38 (2015) 1700–1706.
[45] M. Chayah, M.D. Carrión, M.A. Gallo, R. Jiménez, J. Duarte, M.E. Camacho, Chem. Med. Chem. 10 (2015) 874–882.
[46] S. Li, X. Sun, Y. Li, F. Liu, J. Ma, L. Tong, G. Su, J. Xu, Y. Ohizumi, D. Lee, Y. Guo, Bioorg. Med. Chem. Lett. 27 (2017) 670–674.